

The William-Wehlau Spectropolarimeter: Observing Hot Stars in All Four Stokes Parameters

THOMAS EVERSBERG,^{1,2} ANTHONY F. J. MOFFAT,^{1,2} MICHAEL DEBRUYNE,^{2,3} JOHN B. RICE,⁴ NIKOLAI PISKUNOV,^{3,5}
PIERRE BASTIEN,¹ WILLIAM H. WEHLAU,^{3,6} AND OLIVIER CHESNEAU⁷

Received 1998 February 13; accepted 1998 July 22

ABSTRACT. We introduce a new polarimeter unit, which, mounted at the Cassegrain focus of any telescope and fiber-connected to a fixed CCD spectrograph, is able to measure all Stokes parameters I , Q , U , and V across spectral lines of bright stellar targets and other point sources in a quasi-simultaneous manner. Applying standard reduction techniques for linearly and circularly polarized light, we are able to obtain photon noise-limited line polarization. We briefly outline the technical design of the polarimeter unit and the linear algebraic Mueller calculus for obtaining polarization parameters of any point source. In addition, practical limitations of the optical elements are outlined. We present first results obtained with our spectropolarimeter for four bright, hot-star targets. We confirm previous results for $H\alpha$ in the bright Be star γ Cas and find linear depolarization features across the emission-line complex C III/C IV (5696/5808 Å) of the WR + O binary γ^2 Vel. We also find circular line polarization in the strongly magnetic Ap star 53 Cam across its $H\alpha$ absorption line. No obvious line polarization features are seen across $H\alpha$ in the variable O star θ^1 Ori C above the $\sigma \sim 0.2\%$ instrumental level.

1. INTRODUCTION

Obtaining polarization spectra of stars is a relatively young topic. Only a few instruments exist for mid- and large-size telescopes—needed to detect the generally low polarization levels. Most popular is the use of a rotatable half-wave retarder plate along with a crystal polarizer to measure linearly polarized light. Examples of where this is done are the Anglo-Australian (Bailey 1989) and Herschel (Tinbergen & Rutten 1992) telescopes. At Keck the so-called “dual-waveplate” method is used (see, e.g., Cohen et al. 1996; Goodrich, Cohen, & Putney 1995) consisting of a quarter-wave and a half-wave plate. Using a quarter-wave plate (QWP), e.g., at ESO/CASPEC, allows one to measure circularly polarized light (Mathys & Stenflo 1976). However, there are only a few instruments able to conveniently

measure both linearly and circularly polarized light together. A very recent example is the new spectropolarimeter at the Bernard Lyot Telescope at Pic Du Midi (Donati et al. 1997).

Some stars are well known to show intrinsic linear (see, e.g., St-Louis et al. 1987) as well as circular (see, e.g., Borra & Landstreet 1980) *continuum* polarization. The main sources of intrinsic continuum polarization are electron (Thomson) and (less important) Rayleigh scattering in stellar atmospheres and environments, whereas nonrelativistic gyrating electrons in magnetic fields yield broadband linear *and* circular polarization (see, e.g., Schmidt 1988). Interstellar grains normally lead to smoothly wavelength-dependent linear polarization (Serkowski, Mathewson, & Ford 1975), with low-amplitude circular polarization crossing over at linear peak (Martin & Campbell 1976). Intrinsic *line* polarization can occur due to the Zeeman effect (circular and, to a lesser extent, linear, depending on the magnetic field strength and orientation) and asymmetries between line and continuum sources (linear). For example, emission lines formed further out in a stellar wind are generally less polarized, leading to linear depolarization across the line if asymmetries such as wind flattening are present (Schulte-Ladbeck, Meade, & Hillier 1992).

Spectropolarimetry is relatively rarely used in stellar astronomy. In this paper we focus on spectropolarimetry of hot stars only, for which the main difficulties are the following:

1. The degree of hot-star (from $T_{\text{eff}} = 7500$ K for an A9

¹ Département de Physique, Université de Montréal, C.P. 6128, Succ. Centre-Ville, Montréal, QC H3C 3J7, Canada, moffat@astro.umontreal.ca; and Observatoire du Mont Mégantic.

² Visiting Astronomer, University of Toronto Southern Observatory, Las Campanas, Chile.

³ Department of Physics and Astronomy, University of Western Ontario, London, ON N6A 3K7, Canada.

⁴ Brandon University, 270-18th Street, Brandon, MB R7A 6A9, Canada.

⁵ Uppsala University, Box 5151, S-751 20 Uppsala, Sweden.

⁶ Deceased.

⁷ Observatoire de la Côte d’Azur, 2130 route de l’Observatoire, Caussols, 06460 St. Vallier de Thiey, France.

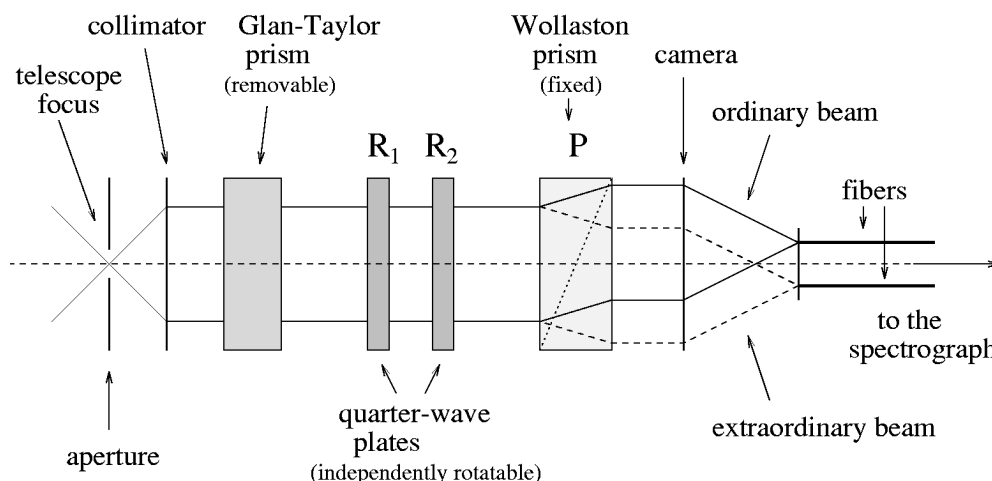


FIG. 1.—Simple sketch of the William-Wehlaau Spectropolarimeter

star to 50,000 K for an O3 star) polarization is often much less than 1% in the continuum, 0.1% in lines (excluding Ap stars) which requires long exposure times and/or large telescopes.

2. If in a stellar atmosphere the source of electron (or Rayleigh) scattering shows radial symmetry, most of the polarization cancels out. As a consequence, deviations from spherical symmetry or a structured wind are the fundamental conditions for detection of intrinsic, nonmagnetic linear polarization.

3. A global stellar magnetic dipole is the field configuration with the highest probability of detection in circular polarization. Detection of higher order or localized dipole field geometries is more difficult, requiring high spectral resolution aided by stellar rotation or wind expansion.

On the other hand, the step from measuring broadband to measuring narrowband (i.e., spectral) polarization allows one to better disentangle the global structure of hot star winds and/or to provide more detailed information about magnetic field geometries. Furthermore, it is of great interest to measure both linear *and* circular polarization at the same (or nearly so) time, since, e.g., in hot stars, the magnetic configuration producing circular line polarization is expected to be associated with wind asymmetries yielding linear polarization. For a more detailed review about the use of spectropolarimetry in hot stars we refer to Eversberg (1996).

2. THE POLARIMETER UNIT AND THE MUELLER CALCULUS

The newly built William-Wehlaau Spectropolarimeter is a combination of a retarder consisting of two rotatable QWPs and a Wollaston prism as beam-splitter and double-beam po-

larizer, leading light from stellar point sources via a double fiber-feed into a fixed CCD slit spectrograph. The instrument was developed and built at the University of Western Ontario in collaboration with Brandon University (Manitoba) and Université de Montréal (Québec). Figure 1 shows the basic design of the polarimeter unit.

The WW Spectropolarimeter performs polarimetric analysis of starlight. It is designed to be mounted at the $\approx f/8$ Cassegrain focus of medium- or large-size telescopes. Incoming starlight passes through an input aperture (pinhole, normally with a diameter $D = 200 \mu\text{m}$) and is collimated by an $f/8$ system of lenses. The collimated light then passes through the analyzing section of the instrument consisting of two rotatable achromatic AR coated QWPs (controlled by a personal computer) and a fixed Wollaston prism as polarizer. The independent rotation of the QWPs relative to the Wollaston prism determines the polarization components that are being measured. The Wollaston prism separates the components into two linearly polarized beams whose polarization orientations are parallel (ordinary ray, I_{\parallel}) and perpendicular (extraordinary ray, I_{\perp}) to the fast axis of the prism.

The two beams exit the Wollaston prism separated by an angle of $0^{\circ}67'$, with each beam deviating the same amount from the optical axis. A zoom lens system then focuses the aperture for each beam to $D = 100 \mu\text{m}$ at $f/4$ onto twin $D = 150 \mu\text{m}$ optical fibers (silica, step-indexed, high OH, polymide buffer), which are separated by 1 mm. Therefore, light that is always $\approx 100\%$ polarized parallel to the fast axis is focused onto one fiber, while light that is always $\approx 100\%$ polarized perpendicular to the fast axis is focused onto the other fiber. Note that a deviation between the orientation axes of the Wollaston prism

and the zero positions of the QWPs is necessary so that this can occur (see below).

The fibers then feed the light for each beam to the slit of a spectrograph, where the $\approx f/4$ emerging light from the fibers is reimaged to $f/8$ at the slit. The spectra of the light from each fiber are imaged so that they are parallel and adjacent, with sufficient space between them on the CCD detector of the spectrograph. The two components can be combined over an observing sequence to obtain all four Stokes parameters, which fully define the polarization of the light. When the light is dispersed by the spectrograph, the polarization of the starlight may be calculated as the wavelength-dependent quantities $I(\lambda)$, $Q(\lambda)$, $U(\lambda)$, and $V(\lambda)$ via the Mueller calculus (see below).

For calibration purposes and locating the zero position of the QWPs,⁸ a removable Glan-Taylor prism, which produces nearly 100% linearly polarized light at all optical wavelengths, can be inserted in front of the retarders. The fast axes of the QWPs must first be aligned with the symmetry axis of the Wollaston prism to obtain simple orientation relations for the polarimetric output. This can be entirely done automatically using a computer algorithm or step by step by rotating each QWP to locate intensity extrema of the 100% polarized beam exiting the Glan-Taylor prism. The polarization axis of the Glan-Taylor prism is normally aligned with the axis of the Wollaston prism. This is necessary to get a simple output for 100% polarized light (maximum in one beam, minimum in the other). The fiber positions are aligned with the Wollaston axis by shining light back through the fibers, whose orientation as well as that of the Wollaston axis is adjusted so that one sees two colinear pairs of beams arriving at the aperture plane (viewed by reflection from behind). The two inner beams of each pair must superimpose onto the aperture for correct alignment.

Following the Mueller calculus and the rules for matrix algebra, we can calculate the four Stokes parameters for this arrangement with retardance τ (ideally 90°) for both QWPs. With \mathbf{A} the input Stokes vector (I , Q , U , V) and \mathbf{A}' the output Stokes vector (I' , Q' , U' , V') after passing the retarder plates with matrices \mathbf{R}_1 and \mathbf{R}_2 , and the polarizer with matrix \mathbf{P} , we have (writing \mathbf{A} and \mathbf{A}' in vertical form)

$$\mathbf{A}' = \mathbf{P} \times \mathbf{R}_2 \times \mathbf{R}_1 \times \mathbf{A}. \quad (1)$$

Note that we can only actually measure intensities I' of the output beams. The general forms of $\mathbf{R}_{1,2}$ and \mathbf{P} (assumed to be

well aligned in the beam) are given by Serkowski (1962):

$$\mathbf{R} = [X_1 \ X_2 \ X_3 \ X_4], \quad (2)$$

where

$$\begin{aligned} X_1 &= \begin{pmatrix} 1 \\ 0 \\ 0 \\ 0 \end{pmatrix}, \\ X_2 &= \begin{pmatrix} 0 \\ \cos^2 2\psi + \sin 2\psi \cos \tau \\ (1 - \cos \tau) \cos 2\psi \sin 2\psi \\ \sin 2\psi \sin \tau \end{pmatrix}, \\ X_3 &= \begin{pmatrix} 0 \\ (1 - \cos \tau) \cos 2\psi \sin 2\psi \\ \sin^2 2\psi + \cos^2 2\psi \cos \tau \\ -\cos 2\psi \sin \tau \end{pmatrix}, \\ X_4 &= \begin{pmatrix} 0 \\ -\sin 2\psi \sin \tau \\ \cos 2\psi \sin \tau \\ \cos \tau \end{pmatrix}, \end{aligned}$$

and

$$\mathbf{P} = \frac{1}{2} \begin{pmatrix} 1 & \cos 2\varphi & \sin 2\varphi & 0 \\ \cos 2\varphi & \cos^2 2\varphi & \cos 2\varphi \sin 2\varphi & 0 \\ \sin 2\varphi & \cos 2\varphi \sin 2\varphi & \sin^2 2\varphi & 0 \\ 0 & 0 & 0 & 0 \end{pmatrix}, \quad (3)$$

where ψ is the rotation angle of the retardation plate axis with respect to the polarizer axis measured counterclockwise as seen looking toward the sky, and φ is the transmission angle of the polarizer ($\varphi = 0^\circ$ for \parallel , $\varphi = 90^\circ$ for \perp).

Following these expressions for different angular positions of the QWPs and adopting $\tau \equiv 90^\circ$ for both plates, we get a number of resulting equations for the final, observed Stokes parameters, of which the intensity I' (after allowance for various gain factors) contains all the information we need to derive I , Q , U , and V of the original beam \mathbf{A} . If we indicate the intensity in either of the detected output beams $I'_{\psi_1, \psi_2, \parallel}$, $I'_{\psi_1, \psi_2, \perp}$, with respect to the angular values of the two retarders, and orientation of the beams from the polarizer (\parallel or \perp), in this order, F is a time-dependent varying function, which is the same for each beam, here F_{ψ_1, ψ_2} (e.g., atmospheric seeing, transparency), and G is the time-independent gain factor for each beam (e.g., fiber

⁸ According to the manufacturer's specifications, the currently installed achromatic QWPs have ideal retardances ($\tau = 90^\circ$) at two wavelengths only, $\lambda = 4300$ and 6000 \AA . Between, and out to several 100 \AA beyond these values, the retardance varies in a simple but nonlinear fashion between 85° and 95° .

transmission, pixel sensitivity), we obtain, for example:⁹

$$I'_{0,0,\parallel} = \frac{1}{2}(I + Q)F_{0,0}G_{\parallel}, \quad (4a)$$

$$I'_{0,0,\perp} = \frac{1}{2}(I - Q)F_{0,0}G_{\perp}, \quad (4b)$$

$$I'_{45,45,\parallel} = \frac{1}{2}(I - Q)F_{45,45}G_{\parallel}, \quad (4c)$$

$$I'_{45,45,\perp} = \frac{1}{2}(I + Q)F_{45,45}G_{\perp}, \quad (4d)$$

$$I'_{0,45,\parallel} = \frac{1}{2}(I + U)F_{0,45}G_{\parallel}, \quad (4e)$$

$$I'_{0,45,\perp} = \frac{1}{2}(I - U)F_{0,45}G_{\perp}, \quad (4f)$$

$$I'_{0,-45,\parallel} = \frac{1}{2}(I - U)F_{0,-45}G_{\parallel}, \quad (4g)$$

$$I'_{0,-45,\perp} = \frac{1}{2}(I + U)F_{0,-45}G_{\perp}, \quad (4h)$$

$$I'_{-45,0,\parallel} = \frac{1}{2}(I + V)F_{-45,0}G_{\parallel}, \quad (4i)$$

$$I'_{-45,0,\perp} = \frac{1}{2}(I - V)F_{-45,0}G_{\perp}, \quad (4j)$$

$$I'_{45,0,\parallel} = \frac{1}{2}(I - V)F_{45,0}G_{\parallel}, \quad (4k)$$

$$I'_{45,0,\perp} = \frac{1}{2}(I + V)F_{45,0}G_{\perp}. \quad (4l)$$

With these equations we easily obtain the intensity-normalized Stokes parameters q , u , and v :

$$q \equiv \frac{Q}{I} = \frac{R_Q - 1}{R_Q + 1}, \quad (5a)$$

$$u \equiv \frac{U}{I} = \frac{R_U - 1}{R_U + 1}, \quad (5b)$$

$$v \equiv \frac{V}{I} = \frac{R_V - 1}{R_V + 1}, \quad (5c)$$

with

$$R_Q = \sqrt{\frac{I'_{0,0,\parallel} I'_{45,45,\perp}}{I'_{0,0,\perp} I'_{45,45,\parallel}}}, \quad (6a)$$

$$R_U = \sqrt{\frac{I'_{0,45,\parallel} I'_{0,-45,\perp}}{I'_{0,45,\perp} I'_{0,-45,\parallel}}}, \quad (6b)$$

$$R_V = \sqrt{\frac{I'_{-45,0,\parallel} I'_{45,0,\perp}}{I'_{-45,0,\perp} I'_{45,0,\parallel}}}. \quad (6c)$$

Note that these double ratios¹⁰ are impervious to both time-dependent variations and time-independent gain factors (no flat-fielding necessary), as long as the two beams are measured simultaneously on the same part of the detector each time. This is normally the case. They should therefore be purely photon-noise limited. The intensity I , within a constant factor (which will vary smoothly with wavelength, as for any spectrograph), is easy to get from a simple addition of both beams on a given image, after appropriate determination of the gain factors by flat-fielding. Since q , u , and v are independent of these gain factors, it is clear that one can obtain much higher precision for them compared to I . Also note that any of the angles ψ of the $\lambda/4$ plates can be replaced by $\psi \pm 180^\circ$ with identical results, providing the surfaces of the plates are not inclined to the optical axis (Serkowski 1974). This is shown in two-dimensional mode in Table 1 for the two QWP position angles ψ_1 and ψ_2 and the corresponding output $I'_{\parallel}/I'_{\perp}$.

If τ deviates from 90° , the matrix \mathbf{R} introduces cross-talk in the output Stokes parameters. In our case, measured values for the output $I'_{\parallel}/I'_{\perp}$ using the Glan-Taylor prism deviate slightly from expected values. This is shown in Table 2, where each matrix element consists of the theoretically expected value above the measured output value $I'_{\parallel}/I'_{\perp}$ in parentheses.

While modern achromatic polarizing elements (e.g., Glan-Taylor prisms, Wollaston prisms) can be manufactured to very high tolerances, the same cannot be claimed for retarders, even if “superachromatic” (V. Vats 1997, private communication). In an attempt to calculate the real retardance for each QWP at a fixed wavelength, we start with

$$\mathbf{A}' = \mathbf{P} \times \mathbf{R} \times \mathbf{A}. \quad (7)$$

Using the Mueller matrices \mathbf{P} and \mathbf{R} , we have for the ordinary beam

$$I'_{\parallel} = \frac{F_{\psi} G_{\parallel}}{2} [I + Q(\cos^2 2\psi + \sin^2 2\psi \cos \tau)$$

$$+ U(1 - \cos \tau) \cos 2\psi \sin 2\psi - V \sin 2\psi \sin \tau], \quad (8a)$$

and for the extraordinary beam

$$I'_{\perp} = \frac{F_{\psi} G_{\perp}}{2} [I - Q(\cos^2 2\psi + \sin^2 2\psi \cos \tau)$$

$$- U(1 - \cos \tau) \cos 2\psi \sin 2\psi + V \sin 2\psi \sin \tau]. \quad (8b)$$

With 100% polarized light in Q (i.e., with the aligned Glan-

⁹ Intermediate QWP positions are also usable, in principle, though requiring more complicated calculations.

¹⁰ This is referred to as self-calibration by Miller et al. (1988).

TABLE 1
OUTPUT MATRIX FOR THE RATIO I_{\parallel}/I_{\perp} AND DIFFERENT QWP POSITIONS

ψ_2	ψ_1							
	-90°	-45°	0°	45°	90°	135°	180°	225°
-180°	$I+Q$ $I-Q$	$I+V$ $I-V$	$I+Q$ $I-Q$	$I-V$ $I+V$	$I+Q$ $I-Q$	$I+V$ $I-V$	$I+Q$ $I-Q$	$I-V$ $I+V$
-135°	$I-U$ $I+U$	$I+Q$ $I-Q$	$I+U$ $I-U$	$I-Q$ $I+Q$	$I-U$ $I+U$	$I+Q$ $I-Q$	$I+U$ $I-U$	$I-Q$ $I+Q$
-90°	$I-Q$ $I+U$	$I+V$ $I-V$	$I+Q$ $I-Q$	$I-V$ $I+V$	$I+Q$ $I-Q$	$I+V$ $I-V$	$I+Q$ $I-Q$	$I-V$ $I+V$
-45°	$I-U$ $I+Q$	$I+Q$ $I-Q$	$I+U$ $I-U$	$I-Q$ $I+Q$	$I-U$ $I+U$	$I+Q$ $I-Q$	$I+U$ $I-U$	$I-Q$ $I+Q$
0°	$I-Q$ $I+U$	$I+V$ $I-V$	$I+Q$ $I-Q$	$I-V$ $I+V$	$I+Q$ $I-Q$	$I+V$ $I-V$	$I+Q$ $I-Q$	$I-V$ $I+V$
45°	$I-U$ $I+U$	$I+Q$ $I-Q$	$I+U$ $I-U$	$I-Q$ $I+Q$	$I-U$ $I+U$	$I+Q$ $I-Q$	$I+U$ $I-U$	$I-Q$ $I+Q$
90°	$I-Q$ $I+U$	$I+V$ $I-V$	$I+Q$ $I-Q$	$I-V$ $I+V$	$I+Q$ $I-Q$	$I+V$ $I-V$	$I+Q$ $I-Q$	$I-V$ $I+V$
135°	$I-U$ $I+Q$	$I+Q$ $I-Q$	$I+U$ $I-U$	$I-Q$ $I+Q$	$I-U$ $I+U$	$I+Q$ $I-Q$	$I+U$ $I-U$	$I-Q$ $I+Q$

NOTES.—Output matrix for the ratio I_{\parallel}/I_{\perp} and different QWP positions according to eqs. (4a)–(4l), generalized to include all useful angles that measure one Stokes polarization parameter at a time, but neglecting G_{\parallel}/G_{\perp} . The QWP angles refer to ideal values ψ , not ψ_{obs} ; see text. Values of ψ do not run from 0° to 360° for each plate, due to limitations in rotation of the QWPs in the WW spectropolarimeter (cf. Table 2).

Taylor prism) we have $U = V = 0$ and $Q = I$, and we get

$$I_{\parallel}' = \frac{F_{\psi} G_{\parallel} I}{2} (1 + \cos^2 2\psi + \sin^2 2\psi \cos \tau) \quad (9a)$$

and

$$I_{\perp}' = \frac{F_{\psi} G_{\perp} I}{2} (1 - \cos^2 2\psi - \sin^2 2\psi \cos \tau). \quad (9b)$$

For $\tau = 90^\circ$, we have the ideal case:

$$I_{\parallel}' = \frac{F_{\psi} G_{\parallel} I}{2} (1 + \cos^2 2\psi) \quad (10a)$$

and

$$I_{\perp}' = \frac{F_{\psi} G_{\perp} I}{2} \sin^2 2\psi. \quad (10b)$$

However, I_{\parallel}' and I_{\perp}' deviate slightly from the expected ideal output functions at certain angular positions. In detail within the constants G_{\parallel} and G_{\perp} , $I_{\parallel}' + I_{\perp}'$ is conserved, whereas maxima of I_{\perp}' and minima of I_{\parallel}' appear to follow a simple sine wave with rotation angle. This behavior must obviously be caused by small deviations of τ from 90° for both QWPs. By using

$$\cos \tau = c_1 + c_2 \sin \psi + c_3 \cos \psi, \quad (11)$$

we fitted equations (9a) and (9b) via χ^2 minimization, leading to $(F_{\psi} G_{\parallel} I/2, F_{\psi} G_{\perp} I/2) = (5303, 4559)$, $c_1 = 0.050$, $c_2 = -0.049$, and $c_3 = -0.001$ for QWP 1 and $(F_{\psi} G_{\parallel} I/2, F_{\psi} G_{\perp} I/2) = (5330, 4700)$, $c_1 = 0.160$, $c_2 = 0.017$, and $c_3 = 0.002$ for QWP 2. The fit also yielded a slight shift of the extrema from their theoretically expected positions, leading to corrections $\psi = 0.994\psi_{\text{obs}} - 10^\circ.12$ for QWP1 and $\psi = 0.999\psi_{\text{obs}} - 13^\circ.87$ for QWP2. The deviation from unity of the

TABLE 2
EXAMPLE OUTPUT MATRIX

ψ_2	ψ_1							
	-90°	-45°	0°	45°	90°	135°	180°	225°
-180°	$\frac{\infty}{(141)}$	$\frac{1}{(0.87)}$	$\frac{\infty}{(66)}$	$\frac{1}{(0.98)}$	$\frac{\infty}{(33)}$	$\frac{1}{(1.09)}$	$\frac{\infty}{(435)}$	$\frac{1}{(0.81)}$
-135°	$\frac{1}{(1.06)}$	$\frac{\infty}{(132)}$	$\frac{1}{(1.52)}$	$\frac{0}{(0.01)}$	$\frac{1}{(0.79)}$	$\frac{\infty}{(73)}$	$\frac{1}{(1.16)}$	$\frac{0}{(0.002)}$
-90°	$\frac{\infty}{(179)}$	$\frac{1}{(0.92)}$	$\frac{\infty}{(109)}$	$\frac{1}{(0.88)}$	$\frac{\infty}{(34)}$	$\frac{1}{(1.14)}$	$\frac{\infty}{(455)}$	$\frac{1}{(0.75)}$
-45°	$\frac{1}{(1.26)}$	$\frac{0}{(0.009)}$	$\frac{1}{(0.85)}$	$\frac{\infty}{(222)}$	$\frac{1}{(1.63)}$	$\frac{0}{(0.027)}$	$\frac{1}{(1.16)}$	$\frac{\infty}{(135)}$
0°	$\frac{\infty}{(476)}$	$\frac{1}{(0.68)}$	$\frac{\infty}{(62)}$	$\frac{1}{(1.15)}$	$\frac{\infty}{(90)}$	$\frac{1}{(0.84)}$	$\frac{\infty}{(370)}$	$\frac{1}{(1.00)}$
45°	$\frac{1}{(0.94)}$	$\frac{\infty}{(204)}$	$\frac{1}{(1.32)}$	$\frac{0}{(0.022)}$	$\frac{1}{(0.69)}$	$\frac{\infty}{(233)}$	$\frac{1}{(1.04)}$	$\frac{0}{(0.008)}$
90°	$\frac{\infty}{(93)}$	$\frac{1}{(1.12)}$	$\frac{\infty}{(556)}$	$\frac{1}{(0.72)}$	$\frac{\infty}{(29)}$	$\frac{1}{(1.36)}$	$\frac{\infty}{(112)}$	$\frac{1}{(0.62)}$
135°	$\frac{1}{(1.20)}$	$\frac{0}{(0.021)}$	$\frac{1}{(0.81)}$	$\frac{\infty}{(667)}$	$\frac{1}{(1.52)}$	$\frac{0}{(0.046)}$	$\frac{1}{(1.15)}$	$\frac{\infty}{(101)}$

NOTES.—Example output matrix with the Glan-Taylor prism inserted ($Q = I, U = V = 0$) for the ratio I_{\parallel}/I_{\perp} and different QWP positions in a narrow band centered near $\text{H}\alpha$. Each matrix element consists of the theoretical output (with $G_{\parallel}/G_{\perp} = 1$) and the measured value in parentheses. Angles have been corrected to coincide with appropriate extrema (ψ , not ψ_{obs} , see Fig. 2).

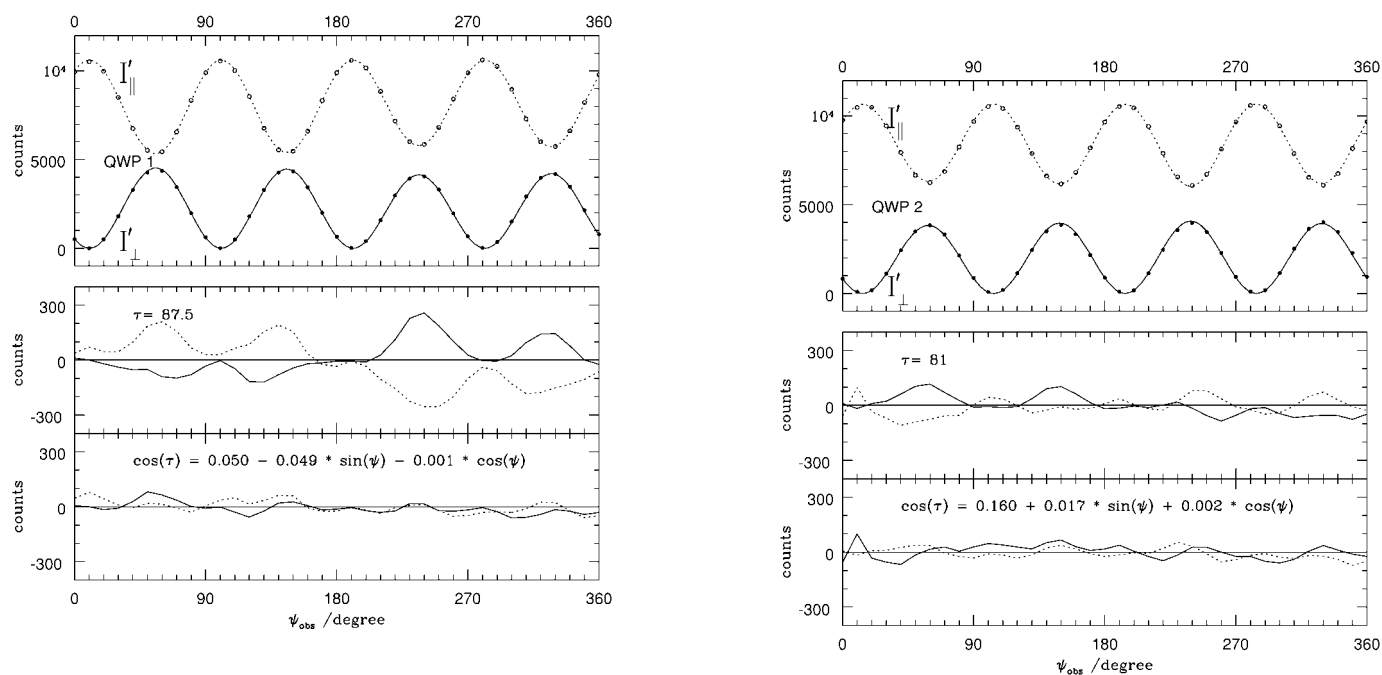


FIG. 2.—Output of the two beams with the Glan-Taylor prism, QWP 1 (*left*) and QWP 2 (*right*) and the Wollaston prism, in a narrow band centered near $H\alpha$. (*Top panel*) Open and filled circles, respectively, represent the measured average intensity in the ordinary beam (I_{\parallel}) and extraordinary beam (I_{\perp}). Curves represent the fits using eqs. (9a), (9b), and (11) after allowing for a shift in angle to match best our data points. (*Bottom panel*) *Top*: residuals from a χ^2 minimum fit for $\tau = \text{constant}$, as indicated for both QWPs. *bottom*: residuals from a χ^2 minimum fit using eq. (11). Values obtained for c_1 , c_2 , and c_3 are indicated.

slopes is likely a consequence of imperfections in the stepping motors.

To illustrate this for the WW polarimeter, we show in Figure 2 for each QWP separately, combined with the aligned Glan-Taylor and Wollaston prisms, how the outputs I_{\parallel} and I_{\perp} vary compared with predictions.

We discovered the reason for this behavior by sending a laser beam through each QWP independently. In transmission, the outgoing beams were geometrically highly stable while rotating the plates, whereas in reflection both plates showed one or two beams that rotated in elliptical patterns around a geometrically stable central beam.

The variation of the effective retardation of the QWPs with rotation angle arises because of the varying angle of inclination that the collimated beam has with the QWP (or one of its individual layers) as the QWP is rotated. If the QWP were mounted in its cell so that the surfaces were not normal to the axis of the cell and the cell axis were properly aligned with the optical axis of the collimated beam, then that one misalignment by itself would produce no change in inclination as the cell is rotated. If the cell were rotated about an axis that is misaligned with the optical axis but the QWP were properly mounted normal to the axis of the cell then again there would be no variation in the inclination angle with rotation as a result of that misalignment alone. However, if both misalignments are present, i.e., the orientation of the QWP in its cell is not normal to the axis of rotation *and* the axis of rotation is not

aligned with the optical axis, then we have an oblique rotator. As the cell is rotated, the angle of inclination will nod with respect to the optical axis and the effective retardation will vary. If the misalignments are only a few minutes of arc, then the variation will be small, of course. In our case we found that the *front* surface of each multielement QWP was normal to the rotation axis of the cell but that the air gap between some of the additional components was a wedge so that some parts of the QWP participated in the oblique rotator behavior. This varying inclination introduces small angle-dependent deviations from the mean retardance (see eqs. [8.3.2] and [8.3.3] in Serkowski 1974). A sine-wave behavior for τ (or $\cos \tau$ for τ moderately close to 90°) is thus quite reasonable, as found above.

The solution to this problem is simple. Either be more careful that there is no misalignment of any of the components of the QWPs in their cells or be careful that the rotation axis is quite precisely aligned with the optical axis. Either will suffice but obviously if both are accomplished the effect we have seen will be removed. It is important to note that we chose to use QWPs with an air gap so that even with variation in the angle of the surfaces of the components to the incident angle of the transmitted beam in a collimated beam situation, there would be absolutely no movement of the image formed by the camera optics. A QWP that is inclined to the collimated beam would produce a displacement of the collimated beam but no deviation in direction. That is a consequence of the fact that a QWP must

have, by its very nature, surfaces that are parallel to one another to a very high degree of precision.

It is not obvious that superachromatic retarders (although giving better tolerances on τ close to 90° , compared to the achromats here) would behave much better (Donati et al. 1997), since they are even more complex, requiring more dielectric layers (V. Vats 1997, private communication).

We also obtained a number of exposures of bright stars with the Glan-Taylor prism to measure the overall efficiency and possible cross-talk between different Stokes parameters at different wavelengths. As seen in Figure 3, cross-talk between different polarization parameters shows wavy structures as a function of wavelength, with an amplitude that never exceeds 4%. Some of the nonzero offset in \bar{u} might be due to a slight misalignment in the rotation of the Glan-Taylor prism. We can, however, exclude this as the reason for the imperfect behavior of retardance τ with angle and wavelength. We find similar behavior also in our UTISO data in the blue.

The bottom line here is that we can probably eliminate these deviations by applying first-order corrections and/or using better QWPs. For our described observations with imperfect QWPs we minimize the impact on deviations in the final Stokes values by choosing ranges of rotation for the QWPs, where the two required ratio peaks are more nearly the same and overall deviations from $\tau = 90^\circ$ are smallest.

3. OBSERVATIONS

In order to test the WW polarimeter on the sky, we have observed a number of different hot star prototypes to cover various spectropolarimetric outputs. These include the brightest Be star visible in the sky γ Cas (B0 IVe), the young variable Orion Trapezium star θ^1 Ori C (O7 V) and the strongly magnetized Ap star 53 Cam (A2p). These were observed during two runs at the 1.6 m telescope of the Observatoire du mont Mégantic (OMM) in 1997 September and December using the William-Wehlau Spectropolarimeter at the Cassegrain focus. With the 600 l/mm grating of the fiber-fed spectrograph we obtained a net (FWHM) resolution of 1.9 \AA in the wavelength range 5800–7100 \AA , to cover mainly H α , He I $\lambda 5876$, and He I $\lambda 6678$.

We have also observed the 78 day WR + O binary γ^2 Vel (WC8 + O9 I) during a five week run in 1997 February/March at the University of Toronto Southern Observatory (UTSO) at Las Campanas, Chile. We obtained spectra during 21 nights within $\Delta\phi \sim \pm 0.2$ of periastron passage. Using the Garrison spectrograph the 3 pixel spectral resolution was about 6 \AA in the effective wavelength region 5200–6000 \AA covering mainly the He II $\lambda 5411$, C III $\lambda 5696$, C IV $\lambda\lambda 5802/12$, and He I $\lambda 5876$ emission lines.

The very first step for each night was the calibration of the QWP positions. For this we sent an artificial light source through the system including the Glan-Taylor prism. With 100% input polarized light, we located where the intensities

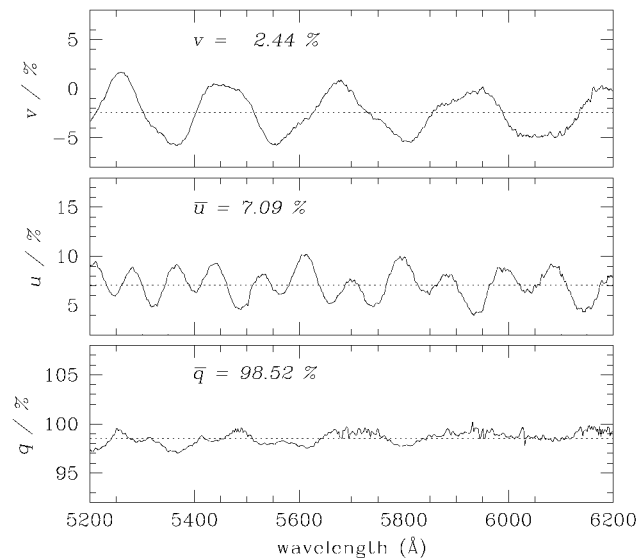


FIG. 3.—Stokes q , u , and v for Sirius (α CMa) observed with the Glan-Taylor prism at UTISO. Average values in the wavelength range 5200–6200 \AA are indicated. Note that v should be zero for a perfect instrument.

I_{\parallel} and I_{\perp} reached extreme values. Actually, our computer program is able to find these extrema by itself. However, we found a small but significant inconsistency in the computer output positions, probably introduced by the chromatic- and angle-dependent nature of the quarter-wave plates.

For each program star we obtained a number of exposure sequences, each containing two, four, or six spectral images at different QWP positions to measure (1) $v(\lambda)$, (2) $q(\lambda)$ and $u(\lambda)$, or (3) $q(\lambda)$, $u(\lambda)$, $v(\lambda)$, respectively, as indicated above (cf. eqs. [4a]–[6c]). One sequence was obtained with the Glan-Taylor prism when necessary, to correct for possible cross-talk between different Stokes parameters and to evaluate the overall efficiency of detecting polarization. Complete sequences for nonpolarized standard stars (e.g., β Cas at OMM and α CMa at UTISO) were also observed. Polarized standards are generally too faint to be observed for our purpose, compounded with a problem of reliably measuring continuum polarization (see below).

A number of flat-field images, wavelength comparison spectra, and bias images were obtained at the beginning and end of each night. The procedures for flat-fielding and wavelength calibration were different at each telescope:

At UTISO we used an internal Tungsten lamp in the optical feeding box between the polarimeter and the telescope for flat-fielding. A Fe-Ne lamp in the same feeding box was used for wavelength calibration.

At OMM we used the auto-guider of the telescope. For this reason we could not use the feeding optics and obtained dome flats in the usual manner. For wavelength calibration we used a Cu-Ar lamp in the spectrograph.

As one can see, light from the comparison lamp at UTISO

passes through the whole instrument, whereas at OMM the comparison light originated in the spectrograph. Despite these different configurations, we found no significant differences between these techniques.

4. DATA REDUCTION

As one can see from the final equations, a full observing sequence for all four Stokes parameters consists of six exposures at different QWP positions. Each exposure results in a two-dimensional CCD image with two spectra, one for the ordinary beam and one for the extraordinary beam.

After bias subtraction, the possibility of blending between the two beams (see Harries 1995 in the case of an echelle spectrograph, where free space between adjacent orders is limited) was considered. Because of ample separation between the two fibers, both where they receive and deliver the light beams, blending is negligible in our case. In addition we checked for any shift of the spectral pair from one image to another on the CCD chip. This is necessary to avoid division by different pixels, and hence different sensitivities on the chip, within the same observing sequence. For this reason we cross-correlated the first image in a given fixed wavelength range with all other images in a direction perpendicular to the dispersion. The shift was always found to be negligibly small.

The next step was to check for deviations from ideal geometrical orientation of the spectra on the CCD chip, in order to avoid problems in tracing the apertures when collapsing the spectra (see Donati et al. 1997). The angle between the dispersion direction and the CCD axis was small: $1^{\circ}0$ at UTSO and $0^{\circ}14$ at OMM. With such small angles, we do not have to worry about significant spectral smearing during the extraction.

The reduction procedure was carried out with IRAF and its standard tools. One problem was the strong asymmetric shape and its slight variation with wavelength of one of the spectrum pairs perpendicular to the dispersion in the UTSO data. The IRAF/APSUM task traces the line peak and averages flux perpendicular to the dispersion direction, so that one might expect glitches in tracing the aperture as the peak shifts along the spectrum. After trying different techniques for the two 10 pixel wide spectra separated center-to-center by about 30 pixels, we decided to choose broad, 30 pixel windows and use the first nightly spectrum as a template for all other spectra in the same night in the same wavelength range, in order to guarantee division always by the same pixels according to equations (6a)–(6c). Note that we have ratioed the two spectra to obtain $q(\lambda)$, $u(\lambda)$, and $v(\lambda)$ after collapsing to one dimension, rather than in the two-dimensional domain. This is quite acceptable (and simplifies the extraction technique), as pointed out below in the context of obtaining $I(\lambda)$. The above procedure was also used for our OMM data, with a window width for collapsing of 30 pixels. We note that tracing the apertures was not a problem here because of symmetric shapes of our two spectra perpendicular to the dispersion.

Cosmic-ray (CR) rejection was done iteratively. At first CRs were identified by eye on the original image and rejected by replacing their intensities by the mean of neighboring unaffected pixels. After collapsing the spectra, any residual spikes in the one-dimensional spectra were deleted by using again the mean of neighboring unaffected pixels after reidentifying them in the two-dimensional input images as cosmic rays. Ratioing the spectra as necessary to obtain q , u , and v has the advantage that cosmic rays, found usually only in one aperture at a time, appear as even stronger, easy to identify spikes relative to the normally uncomplicated q , u , v spectra, after double-ratioing.

We also subtracted the image background, consisting mostly of dark current, which was extremely small compared to the stellar source. For this, we used a median grid of 5 pixels in windows of 10 pixel width centered at 25 pixels on either side of each beam and a background fit in the dispersion direction of third order. The background level increases linearly with exposure time. This also applies to the OMM data, but with a background window of 30 pixel width.

As a final test we extracted the spectra by using simple averages of image windows independent of IRAF/APSUM. We calculated a 20 pixel wide average on the spectra and subtracted 10 pixel wide background averages on both sides of each beam. There is no significant difference between this and the IRAF result. For this reason we took the easy route by extracting all the spectra in one step within IRAF.

Because $I(\lambda)$ cannot be obtained from double ratios as can q , u , and v , but must be obtained from simple additions of two spectra in one image, we are obliged to reduce pixel-to-pixel variations $I'(\lambda)$ by flat-fielding. This reduction step was done after collapsing the flats to one-dimensional spectra using the same nightly template as for starlight. This is possible because the two beams always have the same *relative* pixel-to-pixel illumination, even always the same $\approx 100\%$ linear polarization input into each of the ordinary and extraordinary beam fibers. The only thing that varies at a given wavelength is the relative intensity of each beam, regardless of the spectral and polarimetric details of the stellar source.

The wavelength calibration was carried out for each beam separately using the same nightly stellar extraction template. This was done *before* double-ratioing the spectra to avoid any shift in wavelength space (e.g., due to the dispersion direction being inclined to the CCD axis) between the two spectra. For best results we determined individual residuals of each arc with respect to its rest wavelength and eliminated strong deviators. A fifth-order Legendre polynomial fit related pixel positions to wavelength. The wavelength drift between comparison spectra taken at the beginning and the end of the night was found to be negligibly small. This is not surprising, in view of the stable configuration with the fiber-fed spectrograph fixed in the dome.

After computing all Stokes parameters for γ^2 Vel we found that the continuum polarization varies from one polarization sequence to the next. Further examination revealed that this occurs for all observed stars and thus must be instrumental in

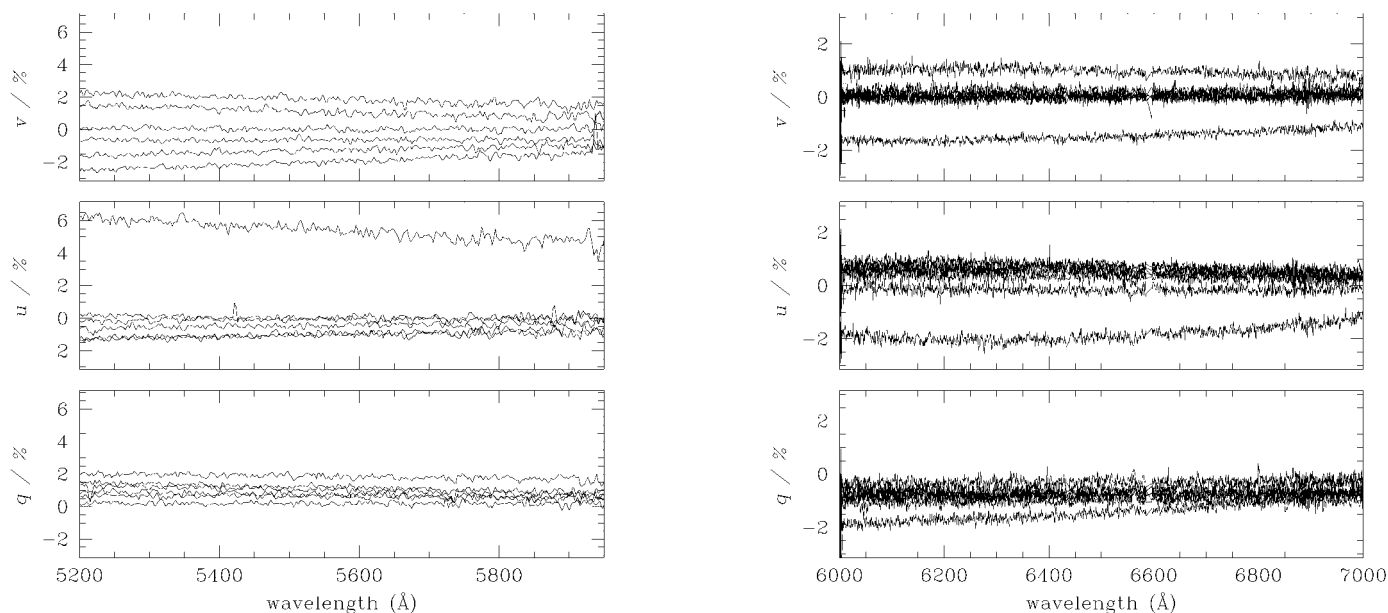


FIG. 4.—(Left) Six consecutive observing sequences of Stokes q , u , and v for γ^2 Vel during one night at UTSO (hand-guided). (Right) Seven consecutive sequences of γ Cas during one night at OMM (auto-guided).

origin. The continuum polarization varies in such a way that strong stochastic deviations from the mean arise, combined with varying gradients $\delta q/\delta\lambda$, $\delta u/\delta\lambda$ and $\delta v/\delta\lambda$. Two examples for consecutive sequences of Stokes q , u , and v obtained at UTSO and OMM are given in Figure 4.

A typical stochastic rms scatter of $\sim 1\%$ broadband contin-

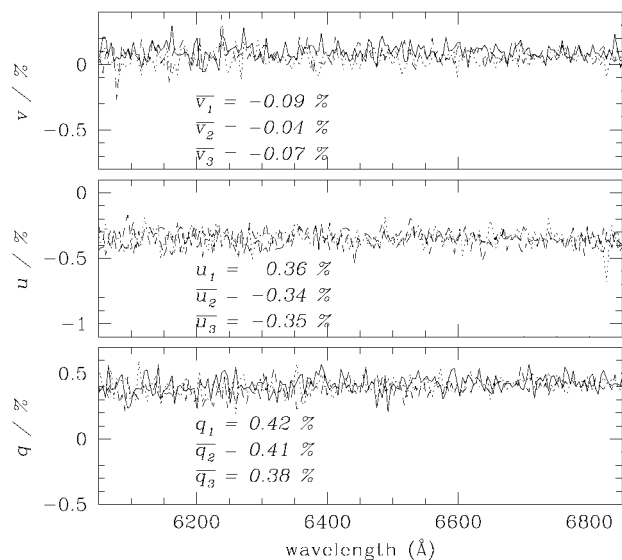


FIG. 5.—Three consecutive observing sequences of Stokes q , u , and v for dome flats at OMM. Average values for q , u , and v in the wavelength range 6050–6850 \AA are indicated. The nonzero means in q and u are likely due to a small level of linear polarization in the dome flat light.

uum polarization is found in q , u , and v at both telescopes. The most likely explanations for this are due to (1) small variations in overall illumination of the two fibers, whose spatial surface sensitivities are never perfectly uniform, and (2) possible metallic aperture edge effects, both caused ultimately by seeing/guiding fluctuations. The first effect dominates in our data, since it appears equally in q , u , and v , whereas the second effect is only expected in q and u . These two effects introduce time dependences in the gain factors, G (see eqs. [4a]–[4l] above) that are different for the two beams. These effects also appear to be worse at blue wavelengths. We believe this is due to wavelength-dependent sensitivity at the fiber-face, which degrades gradually toward shorter wavelengths, as is well known for fiber transmission. Note that at OMM we used the auto-guider, whereas at UTSO guiding was done by eye, leading to somewhat better results at OMM. We find support for the assumed instrumental origin of this scatter by obtaining all Stokes parameters for dome flats, which illuminate the fibers more uniformly and invariably with time. As one can see in Figure 5, the broadband output is stable within $\sim 0.04\%$, i.e., the Poisson noise level.

Donati et al. (1997) have had the same experience with their twin fiber-fed spectropolarimeter. This appears to be a general limitation of such double-fiber configurations. In our polarimeter the pinhole-aperture is imaged onto the fibers. A possible (but difficult) way to avoid variations in broadband polarization could be via imaging of a pupil instead of the star onto the fibers, using Fabry lenses, and via use of a nonmetallic aperture.

As a starting point to circumvent the problem of instrumental variations in continuum polarization, we applied a weighted

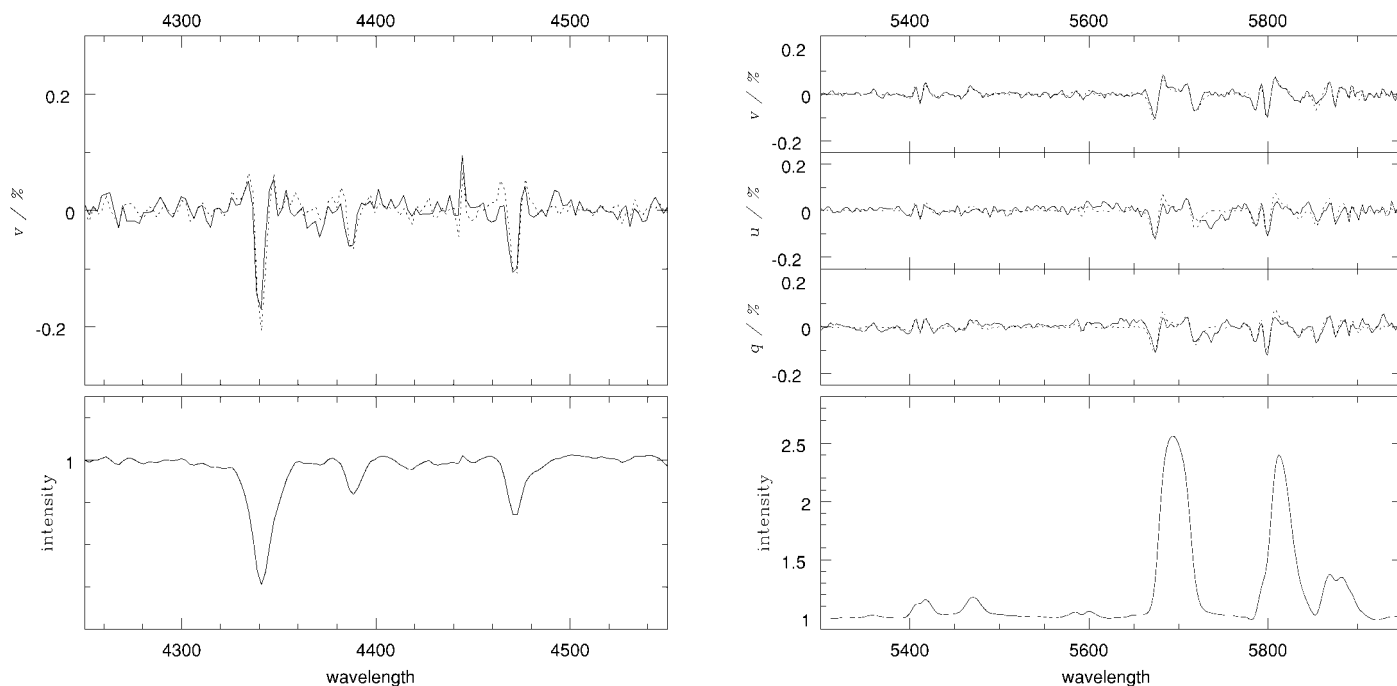


FIG. 6.—Simulation of polarization features with artificially broadened spectra, S_λ (see text). (Left) Bottom: mean spectrum of η Cen. Top: Stokes v (solid line) and S_λ (dashed line). (Right) Bottom: mean spectrum of γ^2 Vel. Top: Stokes q , u , and v (solid line) and S_λ (dashed line).

linear fit to all UTSO $q(\lambda)$, $u(\lambda)$, $v(\lambda)$ spectra, yielding a slope and zero point, neglecting interstellar polarization. (For the OMM data we used a parabolic fit.) Along with other observations, the data in Figure 4 give the impression that the curves tend to converge to the red. In fact, we found a fairly clear correlation between the slopes and their corresponding zero points. However, when applied to the data, the noise of this correlation would introduce continuum variations of up to 2%, which is not acceptable. Thus, we cannot estimate the exact continuum polarization. For this reason we simply subtracted a fit to the original individual Stokes q , u , and v spectra in each sequence and thus neglected broadband polarization, when combining sequences to get mean $q(\lambda)$, $u(\lambda)$, and $v(\lambda)$ spectra. This procedure allows us to obtain reliable, empirical estimates of the *scatter* in polarization as a function of wavelength. On the other hand, *small-scale relative variations of polarization with wavelength* (i.e., *line polarization*), the main goal of this instrument, are impervious to this broadband effect.

After combining to average q , u , and v spectra for various stars of the whole UTSO run, we found Mexican-hat features at atomic line positions in *all* observed absorption lines in *all* Stokes spectra. The amplitude was typically $\sim 0.1\%$ polarization for narrow absorption lines of depth ~ 0.9 continuum. This is small but quite significant and difficult to see even in *nightly* mean spectra. Apparently, the beam that contains enhanced intensity ($I + Q$, $I + U$, $I + V$)—even for $q = u = v = 0$ —broadens the stellar spectrum, regardless of whether in the ordinary beam or in the extraordinary beam. This induces ar-

tificial features in Stokes q , u , and v at wavelengths where the intensity spectra have strong gradients $\delta I / \delta \lambda$. The origin of this behavior is completely unknown. It is not intrinsic to the stars, since it occurs in all lines the same way in q , u , v . If it were due to the spectrograph, it should have cancelled out in the double ratio in equations (6a)–(6c), which is not the case. We first presumed that one or both of the QWPs introduce this phenomenon. However, these features do not appear in our OMM data and it is more likely that our setup at UTSO introduced this behavior in a way that lacks an obvious explanation.

In an attempt to eliminate this effect in the UTSO data, we convolved the mean intensity spectrum I_λ with a Gaussian G_λ containing σ as a free parameter. From this we obtained a modified spectrum S_λ :

$$S_\lambda = \frac{I_\lambda}{I_\lambda \otimes G_\lambda}. \quad (12)$$

This function gives the form of a Mexican hat for narrow lines and resembles the observed spurious line polarization very well. We obtained a best fit with $\sigma = 0.37$ pixel (~ 0.68 Å) for all stars. Examples of this procedure are given in Figure 6.

After subtraction of S_λ from individual nightly mean Stokes spectra at UTSO, we obtained the final wavelength-dependent Stokes parameters $q(\lambda)$, $u(\lambda)$, and $v(\lambda)$. To increase the precision without significant loss in resolution we binned all Stokes

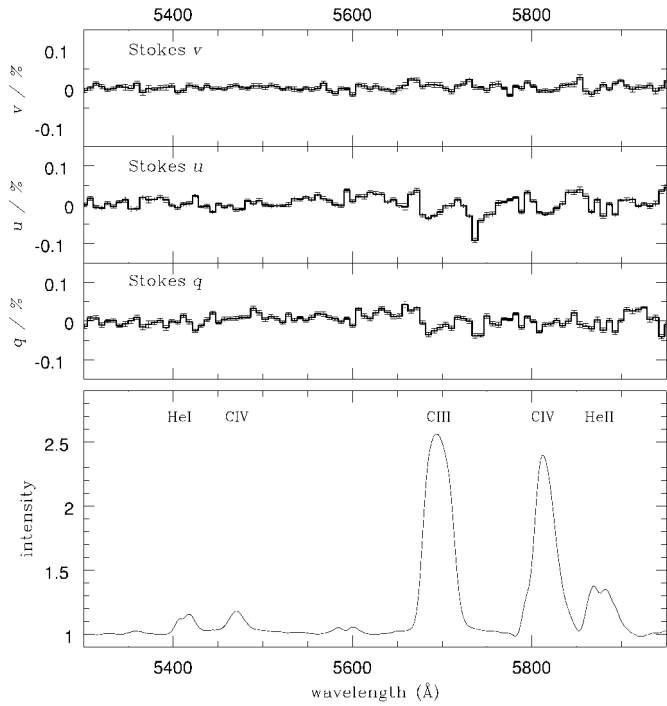


FIG. 7.—Mean rectified intensity spectrum of γ^2 Vel and mean normalized Stokes parameters q , u , and v for the whole run combined, after removal of the spectral broadening effect. The polarimetric data have been binned by a 3 pixel boxcar; 2σ error bars are indicated.

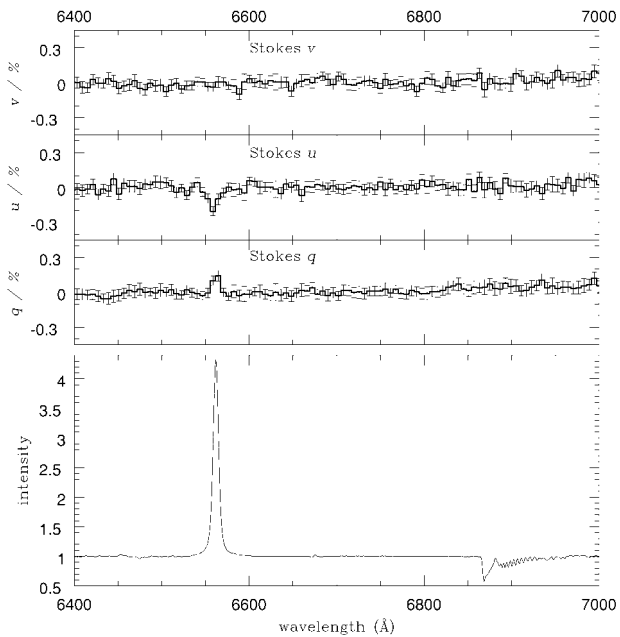


FIG. 8.—Global mean rectified intensity spectrum including $H\alpha$, and mean Stokes q , u , and v for γ Cas; 2σ error bars are indicated for bins of 5 pixels.

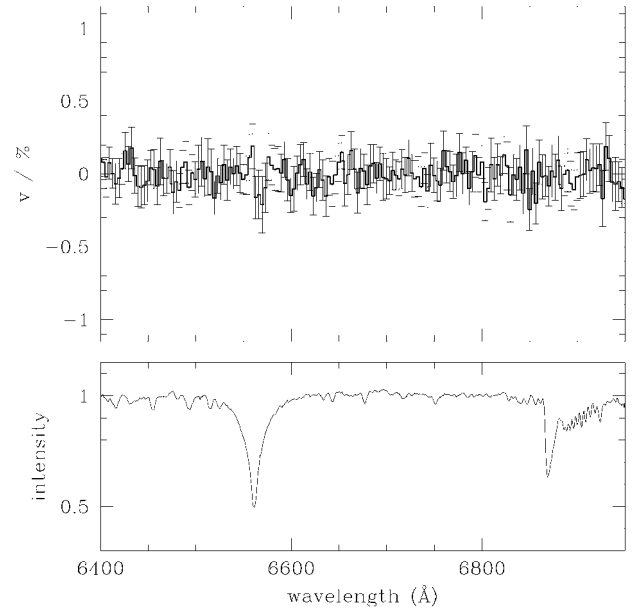


FIG. 9.—Mean rectified intensity spectrum of 53 Cam and mean normalized Stokes v for December 21. The polarimetric data have been binned to 5 pixels; 2σ error bars are indicated.

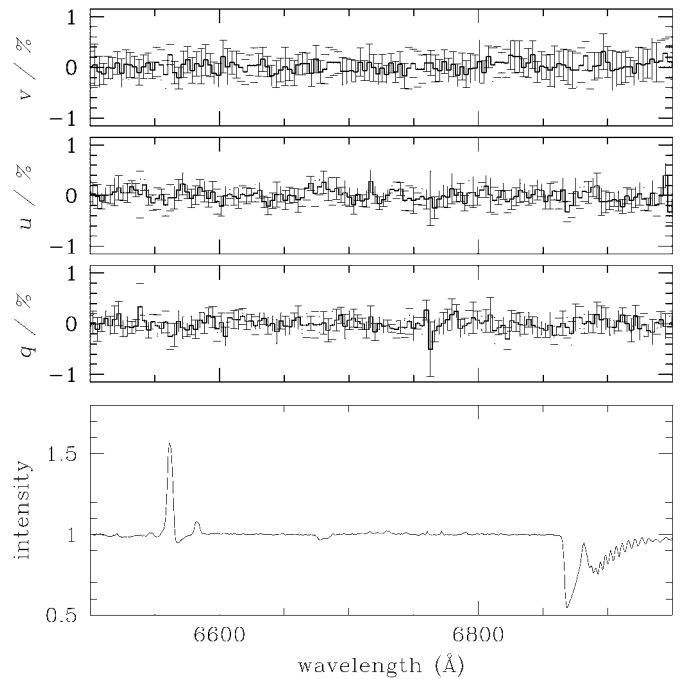


FIG. 10.—Mean rectified intensity spectrum including $H\alpha$, and mean Stokes q , u , and v for θ^1 Ori C; 2σ error bars are indicated for bins of 5 pixels.

spectra to an effective resolution of 2 \AA for the OMM data and 6 \AA for the UTSO data.

5. RESULTS

5.1. γ^2 Velorum

As noted in § 3, spectropolarimetric data of γ^2 Vel were obtained during an extended run at UTSO in 1997 February/March. In this nearby binary system with an orbital period of 78.5 days (Schmutz et al. 1997, who also give a complete description of the orbit), the two wind components create a shock cone around the weaker wind O star (St-Louis, Willis, & Stevens 1993). The variable excess emission in the lines of C III $\lambda 5696$ and C IV $\lambda 5808$ are presumed to be created by radiative cooling downstream along the cone. The opening angle of the cone depends on the relative wind momentum fluxes of the two stars. This shock cone introduces a deviation from spherical symmetry in the wind so that, in principle, it could lead to phase-dependent intrinsic continuum polarization. Even more important to create phase-dependent continuum polarization, however, is the scatter of O-star light from free electrons in the asymmetrically located WR wind (see St-Louis et al. 1988 for γ^2 Vel and other WR + O binaries). On the other hand, WR emission-line flux in a binary will be essentially unpolarized, so that phase-dependent variations of depolarization will occur at the positions of the emission lines (see Moffat & Piirola 1994). We note that constant linear line depolarization can also occur for a flattened WR wind (Schulte-Ladbeck et al. 1992).

Our observations were carried out over orbital phases centered on periastron passage, i.e., $\phi = 0.0 \pm 0.2$. Figure 7 shows all four obtained Stokes parameters I , q , u , and v , averaged over the whole run.

Orbital phase effects have probably diluted the net line polarization, which is expected to be largest at orbital phases when the stars are seen at quadrature. Unfortunately, individual nightly mean spectra are not of sufficient S/N to extract this information. We report significantly different values in both Stokes q and u across strong emission lines compared to the continuum. Since γ^2 Vel is known to show phase-dependent broadband polarization, especially near periastron (St-Louis et al. 1988), it is reasonable to assume that we are seeing line depolarization effects here. We draw attention to additional linear depolarization in the electron scattering (redward) wing of C III $\lambda 5696$.

We find no significant circular polarization across any lines along the whole mean spectrum, above the instrumental level of $\sim 0.03\%$.

5.2. γ Cassiopeiae

We have observed γ Cas during three nights in 1997 September at the mont Mégantic Observatory. γ Cas is one of the best stellar candidates to test for (relatively strong) linear line polarization and our initial goal was to make a comparison with

previous observations. This star is well known to show linear depolarization over its H α line (Poeckert & Marlborough 1977). This is explained by an extended equatorial disk (Hanuschik 1996) that scatters and linearly polarizes photospheric light, combined with the emission of nonpolarized light from recombination lines (Schulte-Ladbeck et al. 1992). γ Cas is also a strong candidate for localized hot flares and magnetic fields (Smith 1998).

Because we are not able to reliably estimate continuum polarization, we can only give relative polarization values across spectral lines. We obtain values for Δq and Δu across H α , equivalent to the values observed some 20 years ago by Poeckert & Marlborough (1977). In Figure 8 we show the three-night average of all four Stokes parameters, with a typical rms scatter of 0.04% for each 5 pixel bin.

5.3. 53 Cam

The Ap star 53 Cam is well known to show an extraordinarily strong effective magnetic field, the strength of which is rotationally modulated between +4 kG and -5 kG, with a corresponding dipole field of -28 kG (Borra & Landstreet 1977). Thus, this star—despite its relative faintness—was our first choice to test our instrument for sensitivity to rotation modulated Stokes v across its photospheric absorption lines. For this reason we observed 53 Cam in the H α region in 1997 December at OMM. Only one night was clear enough to observe this star over a sufficiently long enough interval (6 hr) to obtain high accuracy in Stokes v . This night was December 21/22 at phase $\phi = 0.41$ (Landstreet 1988) after crossover. The average intensity and Stokes v spectra are shown in Figure 9.

Though 1σ error bars are about 0.1% in Stokes v , we report significant rise and fall of $\sim 0.15\%$ on the blue and red sides, respectively, of the center of H α , as expected at this phase from previous work (Borra & Landstreet 1980).

5.4. θ^1 Ori C

The brightest star in the Orion trapezium is the O7 V star θ^1 Ori C. This star, one of the closest O stars in the sky, is the principle ionization source of M42 and spectroscopically variable in the optical (Conti 1972; Walborn 1981) as well as in the UV (Walborn & Panek 1984). Stahl et al. (1993) and Walborn & Nichols (1994) report an asymmetry in its wind and a stable 15.4 day modulation over at least 15 years. They conclude that this behavior is reminiscent of a magnetic oblique rotator with a surface field of about 1800 G. Reported X-ray modulation in the 15 day cycle (Gagné et al. 1997; Babel & Montmerle 1997) is compatible with a surface field of several 100 G. This proposed magnetic field and the wind asymmetry makes θ^1 Ori C a strong candidate for showing phase-dependent circular as well as linear polarization effects across its lines.

We observed this star during two nights (December 21/22 and 22/23) at OMM. The average intensity and Stokes q and u (second night only) and v (1st night only) spectra are shown

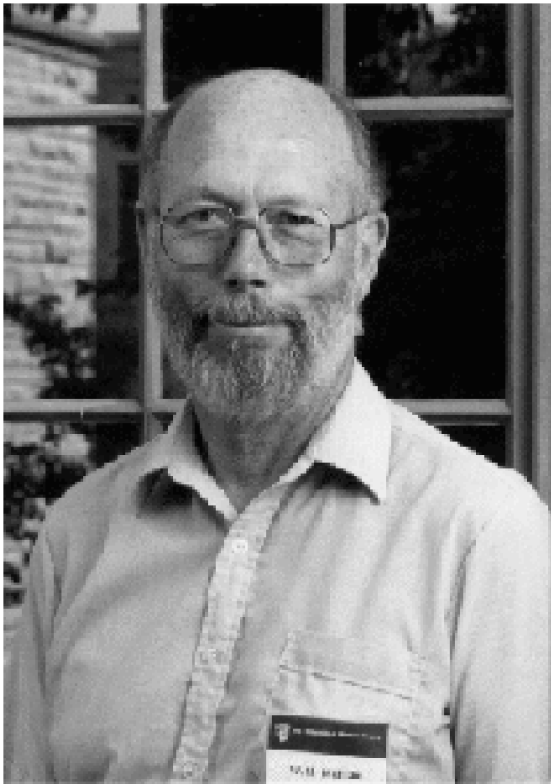


FIG. 11.—William H. Wehlau (1926–1995)

in Figure 10. Note that the nebular $H\alpha$ emission in $I(\lambda)$ has not been removed.

No obvious line polarization features are seen above the $\sigma \sim 0.2\%$ instrumental level.

6. SUMMARY

We have introduced a new type of polarimeter unit, which, mounted at the Cassegrain focus of any telescope and combined with a standard CCD spectrograph, is able to measure all four Stokes parameters as a function of wavelength in a quasi-simultaneous manner. The combination of two independently rotatable quarter-wave plates with a Wollaston polarizer as beam splitter creates a double beam that contains all polarimetric information about the stellar target. An extraction technique is devised that leads to spectra in q , u , and v , whose precision is limited only by stochastic photon noise (Poisson errors), whereas intensity spectra are limited by flat-field noise. We also describe different deviations from ideal for the optical elements. We discuss the behavior of “achromatic” QWPs with respect to chromatism and rotation position, as well as limitations in the use of optical fibers.

During three extended runs at two different telescopes we obtained polarimetric spectra for all four Stokes parameters of several hot star prototypes with the new William-Wehlau Spectropolarimeter. Despite some instrumental problems, we see both line linear depolarization due to Thomson scattering and circular polarization due to Zeeman splitting.

1. For the WR + O binary γ^2 Vel we report polarization features across its strong emission lines. Schulte-Ladbeck et al. (1992) showed that this is due either to a flattened WR wind and/or phase-dependent asymmetries between the O-star and the scatterers mainly in the WR wind.

2. We confirm previously measured polarization variations across the $H\alpha$ emission line of the brightest Be star visible in the sky γ Cas, but with higher precision.

3. We detect a circular polarization feature in $H\alpha$ in the strong magnetic Ap star 53 Cam.

4. For the bright Trapezium star θ^1 Ori C we fail to find any polarization feature in $H\alpha$ at the 0.2% level. Future attempts will have to improve on this precision and secure better phase coverage.

These results establish the William-Wehlau Spectropolarimeter as a viable new instrument for measuring all wavelength-dependent Stokes parameters of stars. Some improvements will be attempted, e.g., better QWPs, dielectric aperture, and more stable illumination of the fibers. Future preference will be given to large telescopes, because of the small amount of polarization in stellar objects.

The authors would like to thank Bob Garrison for the generous allotment of observing time at UTSO, Steve Steeles for his continuous support during observations at UTSO, as well as Bernard Malenfant, Ghislain Turcotte, and Johannes Vorberg at OMM, and Henry Leparskas at Elginfield Observatory. We thank John Landstreet and René Racine for helpful discussions during the development of our instrument, and Jean-François Bertrand for help in Fortran programming. T. E. is grateful for full financial aid from the Evangelisches Studienwerk/Germany, which is supported by the German Government. A. F. J. M., P. B., and J. B. R. thank NSERC (Canada) for financial assistance. A. F. J. M. and P. B. also acknowledge monetary aid from FCAR (Québec).

T. E., A. F. J. M., M. D., J. B. R., N. P., and P. B. wish to note that the original principal investigator for this instrument, William H. Wehlau, unfortunately passed away in 1995 February while attending a scientific meeting in Cape Town, South Africa. We wish to express our deepest respect for his high level of competence and leadership during the planning and early construction stages of the spectropolarimeter that now carries his name (Fig. 11).

REFERENCES

- Babel, J., & Montmerle, T. 1997, *ApJ*, 485, L29
- Bailey, J. 1989, in *Spectropolarimetry at the AAT* (The AAT User's Manual No. 24) (Epping: Anglo-Australian Obs.)
- Borra, E. F., & Landstreet, J. D. 1977, *ApJ*, 212, 141
- . 1980, *ApJS*, 42, 421
- Cohen, M. H. 1996, *Keck User's Manual* (Pasadena: Caltech)
- Conti, P. S. 1972, *ApJ*, 174, L79
- Donati, J.-F., Semel, M., Carter, B. D., Rees, D. E., & Cameron, A. C. 1997, *MNRAS*, 291, 658
- Eversberg, T. 1996, *Hot Star Newslett.* 33
- Gagné, M., Caillault, J.-P., Stauffer, J. R., & Linsky, J. L. 1997, *ApJ*, 478, L87
- Goodrich, R. W., Cohen, M. H., & Putney, A. 1995, *PASP*, 107, 179
- Hanuschik, R. W. 1996, *A&A*, 308, 170
- Harries, T. J. 1995, Ph.D. thesis, University College, London
- Landstreet, J. D. 1988, *ApJ*, 326, 967
- Martin, P. G., & Campbell, B. 1976, *ApJ*, 208, 727
- Mathys, G., & Stenflo, J. O. 1986, *A&A*, 168, 184
- Miller, J. S., Robinson, L. B., & Goodrich, R. W. 1988, in *Instrumentation for Ground-based Astronomy*, ed. L. B. Robinson (New York: Springer), 157
- Moffat, A. F. J., & Piirola, V. 1994, *ApJ*, 413, 724
- Poekert, R., & Marlborough, J. M. 1977, *ApJ*, 218, 220
- Schmidt, G. D. 1988, in *Polarized Radiation of Circumstellar Origin*, ed. G. V. Coyne, A. M. Magalães, A. F. J. Moffat, R. E. Schulte-Ladbeck, S. Tapia, & D. T. Wickramasinghe (Vatican City: Vatican Obs.), 85
- Schmutz, W., et al. 1997, *A&A*, 328, 219
- Schulte-Ladbeck, R. E., Meade, M., & Hillier, D. J. 1992, in *ASP Conf. Ser. 22, Nonisotropic and Variable Outflow from Stars*, ed. L. Drissen, C. Leitherer, & A. Nota (San Francisco: ASP), 118
- Serkowski, K. 1962, in *Adv. Astron. Astrophys.*, 1, 247
- . 1974, in *Methods of Experimental Physics*, Vol. 12, *Astrophysics* (New York: Academic), chap. 8
- Serkowski, K., Mathewson, D. L., & Ford, V. L. 1975, *ApJ*, 196
- Smith, M. 1998, *ApJ*, in press
- Stahl, O., Wolf, B., Gäng, Th., Gummersbach, C. A., Kaufer, A., Kovacs, J., Mandel, H., & Szeifert, Th. 1993, *A&A*, 274, L29
- St-Louis, Drissen, L., Moffat, A. F. J., & Bastien, P. 1987, *ApJ*, 322, 870
- St-Louis, Moffat, A. F. J., Drissen, L., Bastien, P., & Robert, C. 1988, *ApJ*, 330, 286
- St-Louis, N., Willis, A. J., & Stevens, I. R. 1993, *ApJ*, 415, 298
- Tinbergen, J., & Rutten, R. 1992, *The WWH User's Manual* (La Palma: Roque de Los Muchachos Obs.)
- Walborn, N. R. 1981, *ApJ*, 243, L37
- Walborn, N. R., & Nichols, J. S. 1994, *ApJ*, 425, L29
- Walborn, N. R., & Panek, R. J. 1984, *ApJ*, 286, 718